RSC Advances

PAPER

Published on 12 October 2026
Licensed under CC-BY-NC 4.0

Check for updates

Cite this: *RSC Adv.*, 2026, **16**, 62304

Sterol-like natural products and other secondary metabolites with antimicrobial and antiplasmodial activities from *Penicillium tanzanicum*

Joseph Tchamgoue, [ab] Bel Youssouf G. Mountessou, [ac] Terence Yocktan D. Yepdjou,[ab] Aron Trucksess, [d] Lasse van Geelen, [d] Kevin Jordan N. Tchoffo,[e] Mariscal Brice T. Tali, [e] Simone Veglianti, [f] Daniele Padula, [f] Ayaz Ahmed, [g] Rainer Kalscheuer [d] and Simeon F. Kouam [*a]

A recent review on *Penicillium* species highlighted steroids as a taxonomic marker of this genus. In the current study, three steroids (**1–3**), an acetophenone (**4**), and thirteen known compounds (**5–17**) were isolated from the solid culture of *Penicillium tanzanicum*, isolated from bull dung. The structures of the compounds were established using extensive spectroscopic and spectrometric analyses (NMR, HRMS) and by comparison with published data. The absolute configurations of steroids **1–3** were determined by electronic circular dichroism (ECD) calculations, confirming their identities as trestione (**1**), formestane (**2**), and oxandrolone (**3**). The crude extract exhibited moderate activity against *Mycobacterium tuberculosis* (MIC = 400 μg mL^{-1}) and significant activity against *Enterococcus faecalis* and *E. faecium* (MIC = 50 μg mL^{-1}). Compounds **8**, **9**, **11**, and **13** displayed weak to moderate antibacterial and antimycobacterial activities against *M. tuberculosis*, *Staphylococcus aureus*, *E. faecalis*, and *E. faecium*, with MIC values ranging from 50 to 100 μg mL^{-1}. Notably, compounds **1** and **2** demonstrated promising antiplasmodial activity against the multi-resistant *Plasmodium falciparum* (*Pf*Dd2) strain, with IC_{50} values of 26.58 and 15.03 μM, respectively, accompanied by low haemolytic effects. These findings underscore the potential of fungi from underexplored ecological niches as sources of new anti-infective leads warranting further optimisation and preclinical evaluation.

Received 26th July 2026
Accepted 4th October 2026

DOI: 10.1039/d6ra06849a

rsc.li/rsc-advances

1. Introduction

The genus *Penicillium* is among the most prolific and widely distributed fungal genera, renowned for the discovery of penicillin from *P. notatum* by Alexander Fleming.[1] With over 550 accepted species,[2] these fungi inhabit diverse environments, including soil, plants, and organic debris. *Penicillium* species are prolific producers of biologically active secondary metabolites.[3,4]

Beyond their historical significance in antibiotic production, *Penicillium* species are a rich reservoir of novel chemical scaffolds. They produce antibiotics, immunosuppressants, cholesterol-lowering agents, and mycotoxins. This diversity underscores their exceptional biosynthetic potential.[5,6] A recent review in the journal *Phytochemistry*[3] highlighted the genus as a source of bioactive and structurally unusual steroids. Despite this recognised potential, the chemical repertoire of many *Penicillium* species remains underexplored, particularly those from unique habitats or understudied phylogenetic lineages. *Penicillium tanzanicum* represents one such underexplored species. A recent investigation highlighted its ability to produce rare isotachin derivatives with promising anti-inflammatory activity.[4] This aligns with broader evidence that endophytic and environmental *Penicillium* strains are rich sources of novel natural products with significant biological and pharmacological potential.[1] Continued chemical investigation of these species is therefore crucial for expanding our understanding of fungal metabolism and for discovering new lead compounds.

[a]*Department of Chemistry, Higher Teacher Training College, University of Yaoundé I, P.O. Box 47, Yaoundé, Cameroon. E-mail: kfogue@yahoo.com*

[b]*Department of Organic Chemistry, Faculty of Science, University of Yaoundé I, P.O. Box 812, Yaoundé, Cameroon*

[c]*Department of Chemistry, Faculty of Science, University of Buea, P.O. Box 63, Buea, Cameroon*

[d]*Institute of Pharmaceutical Biology and Biotechnology, Heinrich Heine University, Universitätsstrasse 1, 40225 Düsseldorf, Germany*

[e]*Laboratory of Phytobiochemistry and Medicinal Plants Study, Faculty of Science, University of Yaoundé I, P.O. Box 812, Yaounde, Cameroon*

[f]*Dipartimento di Biotecnologie, Chimica e Farmacia, Università di Siena, via A. Moro 2, Siena, 53100, Italy*

[g]*H.E.J. Research Institute of Chemistry, International Centre for Chemical and Biological Sciences (ICCBS), University of Karachi, Karachi-75270, Pakistan*

© 2026 The Author(s). Published by the Royal Society of Chemistry

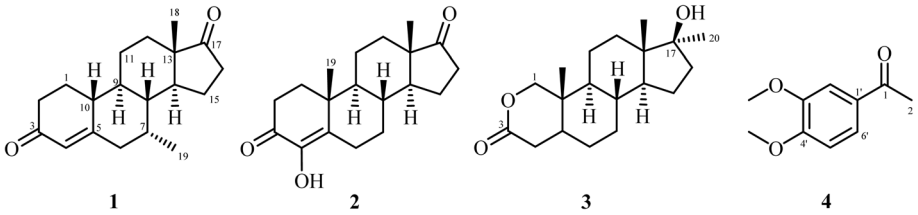


Fig. 1 Structures of compounds 1–4.

In our continuous search for biologically active ingredients from underexplored fungal sources,[7,8] we investigated the chemical constituents of *Penicillium tanzanicum*. This study led to the isolation of three pharmaceutically established steroid drugs, trestione (**1**), formestane (**2**), and oxandrolone (**3**) (Fig. 1). Additionally, a naturally occurring acetophenone (**4**), and thirteen known compounds (**5–17**) were isolated (Fig. S1). The structures of all isolates were elucidated through comprehensive spectroscopic and spectrometric analyses. The discovery that these therapeutically established molecules are natural products biosynthesised by a single fungal strain underscores the potential of the *Penicillium* genus as a prolific source of potent compounds. In addition, the antimicrobial activities of the purified compounds were investigated. The antiplasmodial properties and haemolytic effects of the three sterol-like natural products were also assessed, revealing their antiplasmodial potential. Collectively, these findings expand the chemical profile of *Penicillium tanzanicum* and reinforce the immense value of exploring under-investigated *Penicillium* species as reservoirs of novel drug leads.

2. Results and discussion

2.1. Structural analysis

Compound **1** was obtained as a white powder from the CH_2Cl_2/MeOH (dichloromethane/methanol) solvent system and is soluble in chloroform. Its molecular formula $C_{19}H_{26}O_2$, consistent with seven degrees of unsaturation, was deduced from the positive-ion mode high-resolution electrospray ionisation mass spectrometry [(+)-HRESIMS] analysis, which displayed a molecular ion peak $[M + H]^+$ at *m*/*z* 287.2004 (calcd for $C_{19}H_{27}O_2$, 287.2006) (Fig. S2). The IR (infrared) spectrum exhibited characteristic absorption bands for alkyl (2966–2854 cm^{-1}), conjugated olefin (1660 cm^{-1}), and carbonyl (1735 cm^{-1}) groups (Fig. S3). These were consistent with previously reported α,β-unsaturated steroidal ketones, including androst-4-ene-3,17-dione and 19-norandrost-4-ene-3,17-dione.[9,10] UV (ultraviolet) maxima bands at λ_{max} 241 nm (Fig. S4) confirmed the presence of the α,β-unsaturated ketone.

Analysis of the ^{1}H NMR spectrum of **1** (Fig. S5) in conjunction with the DEPT-HSQC (distortionless enhancement by polarisation transfer–heteronuclear single quantum coherence) spectrum (Fig. S7) revealed in the up-field region signals for a one-olefinic proton singlet at δ_H 5.84; five aliphatic methine protons at δ_H 2.11 (1H, m), 2.04 (1H, m), 1.67 (1H, ddd, $J = 10.8$, 7.2, 3.6 Hz), 1.40 (1H, ddd, $J = 7.2$, 6.0, 5.4 Hz), and 1.15 (1H, dddd, $J = 10.8$, 9.0, 6.6, 4.2 Hz); seven diastereotopic methylene protons in the range δ_H 2.49–1.24; and two methyl proton signals at δ_H 0.92 (3H, s) and 0.80 (3H, d, $J = 7.2$ Hz). These data suggested compound **1** as structurally similar to previously reported steroidal ketones, including androst-4-ene-3,17-dione and estr-4-en-3,17-dione.[11] The ^{13}C NMR spectrum (Fig. S6) revealed 19 distinct carbon resonances which were sorted out using the DEPT-HSQC (Fig. S7) spectrum into two ketonic carbonyl carbons at δ_C 220.3 (C-17) and 199.4 (C-3); two olefinic carbons at δ_C 164.1 (C-5) and 126.8 (C-4); five methine carbons at δ_C 47.1 (C-14), 42.9 (C-10), 42.3 (C-8), 42.2 (C-9), and 30.1 (C-7); seven methylene carbons at δ_C 43.2 (C-6), 36.6 (C-2), 35.6 (C-16), 31.2 (C-12), 26.8 (C-1), 26.2 (C-11), and 21.1 (C-15); two methyl carbons at δ_C 13.7 (C-18) and 12.8 (C-19); and one aliphatic quaternary carbon at δ_C 47.7 (C-13) (Table 1). The HMBC (heteronuclear multiple bond correlation) spectrum (Fig. S8) revealed that the two methyl groups (C-18 and C-19) were attached to C-13 and C-7, respectively. This was evidenced by key correlations between the proton signal at δ_H 0.92 (H-18) and carbons C-17, C-13, and C-12, as well as between the proton signal at δ_H 0.80 (H-19) and carbons C-6, C-7, and C-8 (Fig. 2). Further key HMBC cross-peaks were observed between the diastereotopic methylene proton signals at δ_H 2.28 and 1.58 (H-1a, H-1b) with carbons C-3, C-5, C-9, and C-10; δ_H 1.92 and 1.53 (H-15a, H-15b) with carbons C-17, C-13, C-16, C-14, and C-8; δ_H 2.49 and 2.31 (H-6a, H-6b) with carbons C-5, C-4, C-9, C-7, C-8, and C-19; and the olefinic proton singlet at δ_H 5.84 (H-4) with carbons C-3, C-5, C-10, and C-2 (Fig. 2). The ^{1}H–^{1}H COSY (correlation spectroscopy) spectrum (Fig. S9) further supported the connectivity. It showed correlations between H-4 and H-6, H-6 and H-7, and between H-8 and H-9, H-14, confirming the steroidal skeleton.

The relative configurations of the chiral centres at C-7, C-8, C-9, C-10, C-13, and C-14 were established using the coupling constants, biogenesis considerations, and NOESY (nuclear Overhauser effect spectroscopy) correlations as follows: (a) on the basis of biogenetic considerations of similar reported compounds, the relative configurations of the chiral centres were assigned as (*R*) at C-8, C-10, C-14, and as (*S*) at C-9 and C-13. This was also supported by large coupling constants between H-8α/H-9β ($J = 10.8$ Hz), H-8α/H-14β ($J = 7.2$ Hz), and H-9β/H-10α ($J = 9.0$ Hz), indicating their *trans*-orientations.[12,13] (b) The relative configuration at C-7 was assigned as (*R*) based on a *cis*-orientation between H-7α/H-8α ($J = 3.6$ Hz). This was further supported by a NOESY correlation between the two protons at δ_H 2.11 (H-7α) and 1.67 ppm (H-8α), respectively

© 2026 The Author(s). Published by the Royal Society of Chemistry

Table 1 ^{1}H and ^{13}C NMR data of compounds **1–3**

	1 [a]		**2** [a]		**3** [b]	
No.	δ_H mult. (J in Hz)	δ_C, type	δ_H mult. (J in Hz)	δ_C, type	δ_H mult. (J in Hz)	δ_C, type
1	2.28 m; 1.58 overlapped	44.1, CH_2	2.01 m; 1.63 m	34.6, CH_2	4.25 d (10.7); 4.00 d (10.7)	82.6
2	2.41 m; 2.24 m	36.6, CH_2	2.52 m; 2.49 dd (6.6, 3.0)	31.7, CH_2	—	—
3	—	199.4, C	—	193.4, C		173.8, C
4	5.84 s	126.8, CH	—	139.1, C	2.49 dd (12.9, 6.0); 2.23 dd (12.9, 6.0)	34.6, CH_2
5	—	164.1, C	—	141.3, C	1.77 m	41.2, CH
6	2.49 overlapped; 2.31 m	43.2, CH_2	3.04 m; 1.99 m	35.7, CH_2	1.45 m; 1.29 m	28.1, CH_2
7	2.11 m	30.1, CH	1.95 overlapped; 1.05 m	29.8, CH_2	1.74 m; 0.95 m	31.9, CH_2
8	1.67 ddd (10.8, 7.2, 3.6)	42.3, CH	1.68 m	34.7, CH	1.48 m	36.9, CH
9	1.15 dddd (10.8, 9.0, 6.6, 4.2)	42.2, CH	0.97 m	54.3, CH	0.89 m	50.8, CH
10	2.04 m	42.9, CH	—	37.8, C	—	35.9, C
11	1.98 m; 1.23 m	26.2, CH_2	1.66 m; 1.39 dddd (9.6, 9.0, 4.2, 3.6)	20.2, CH_2	1.51 m; 1.37 m	22.2, CH_2
12	1.80 m; 1.27 m	31.2, CH_2	1.84 m; 1.24 overlapped	31.3, CH_2	1.53 m; 1.31 m	32.5, CH_2
13	—	47.7, C	—	47.5, C	—	46.7
14	1.40 ddd (7.2, 6.0, 5.4)	47.1, CH	1.26 overlapped	50.9, CH	1.23 overlapped	51.7, CH
15	1.92 m; 1.53 m	21.1, CH_2	1.96 m; 1.54 m	21.7, CH_2	1.59 m; 1.29 m	24.2, CH_2
16	2.47 m; 2.09 m	35.6, CH_2	2.45 m; 2.08 m	22.7, CH_2	1.83 m; 1.65 m	39.1, CH_2
17	—	220.3, C	—	220.6, C	—	82.2, C
18	0.92 s	13.7, CH_3	0.89 s	13.7, CH_3	0.85 s	14.6, CH_3
19	0.80 d (7.2)	12.8, CH_3	1.18 s	17.1, CH_3	1.00 s	10.3, CH_3
20	—	—	—	—	1.17 s	26.2, CH_3
4-OH	—	—	6.08 s	—	—	—

[a] Recorded in $CDCl_3$ (^{1}H: 600 MHz; ^{13}C: 150 MHz). [b] Recorded in CD_3OD (^{1}H: 600 MHz; ^{13}C: 150 MHz).

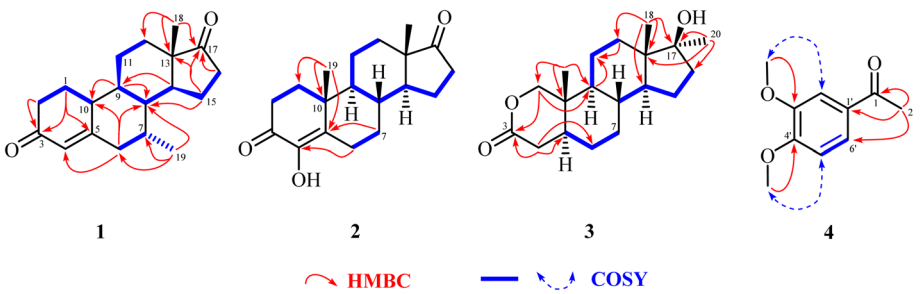


Fig. 2 Key HMBC and ^{1}H–^{1}H COSY correlations for compounds **1–4**.

(Fig. S10 and 2). This NOESY correlation, distinct from ^{1}H–^{1}H COSY connectivity, confirmed their spatial proximity on the same face of the ring system. The *cis*-orientations of H-8 with both H-10 and H-18 were established by NOESY correlations observed between the proton signals at 1.67 (H-8α) and both the signals at δ_H 2.04 (H-10α) and δ_H 0.92 (H-18). Furthermore, the NOESY spectrum exhibited cross-peaks between the methyl protons H-19 (δ_H 0.80) and the methine protons H-9 (δ_H 1.15) and H-14 (δ_H 1.40), establishing their *cis*-orientations. Additional key NOESY correlations are shown in Fig. 3. Hence, the relative configurations were assigned as (7*R*,8*R*,9*S*,10*R*,13*S*,14*S*). The proposed structure was fully supported by HMBC, ^{1}H–^{1}H COSY, and NOESY correlations, as illustrated in Fig. 2 and 3.

The absolute configuration of compound **1** was determined by comparison of its experimental ECD (electronic circular dichroism) spectrum with TDDFT (time-dependent density functional theory)-calculated spectra for both enantiomers of the assigned relative configuration using the protocol described in Section 3.5. Conformational analysis using the CREST (conformer-rotamer ensemble sampling tool) program (300 K, 6 kcal mol^{-1} energy window) identified two major conformers for compound **1**, with Boltzmann populations of 89.58% and 10.42% at 298 K based on DFT-computed Gibbs free energies [B3LYP-D3BJ/def2-TZVP, PCM (polarisable continuum model)/methanol]. The Boltzmann-weighted ECD spectrum, calculated at the TDDFT/B3LYP-D3BJ/def2-TZVP level (16 excited states, σ = 0.30 eV), showed excellent agreement with the experimental spectrum for the (7*R*,8*R*,9*S*,10*R*,13*S*,14*S*) enantiomer (Fig. 4A and S11). It reproduced both the sign and position of the diagnostic negative Cotton effect near 320 nm and the overall spectral profile. The opposite enantiomer gave a mirror-image spectrum that did not match. This assignment was further supported by the good agreement between the calculated (+97.1) and experimental (+66.8) optical rotation

© 2026 The Author(s). Published by the Royal Society of Chemistry

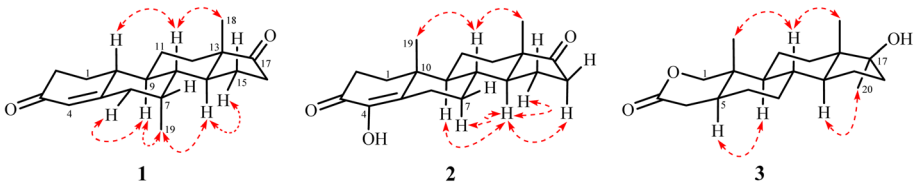


Fig. 3 Key NOESY correlations for compounds **1**–**3**.

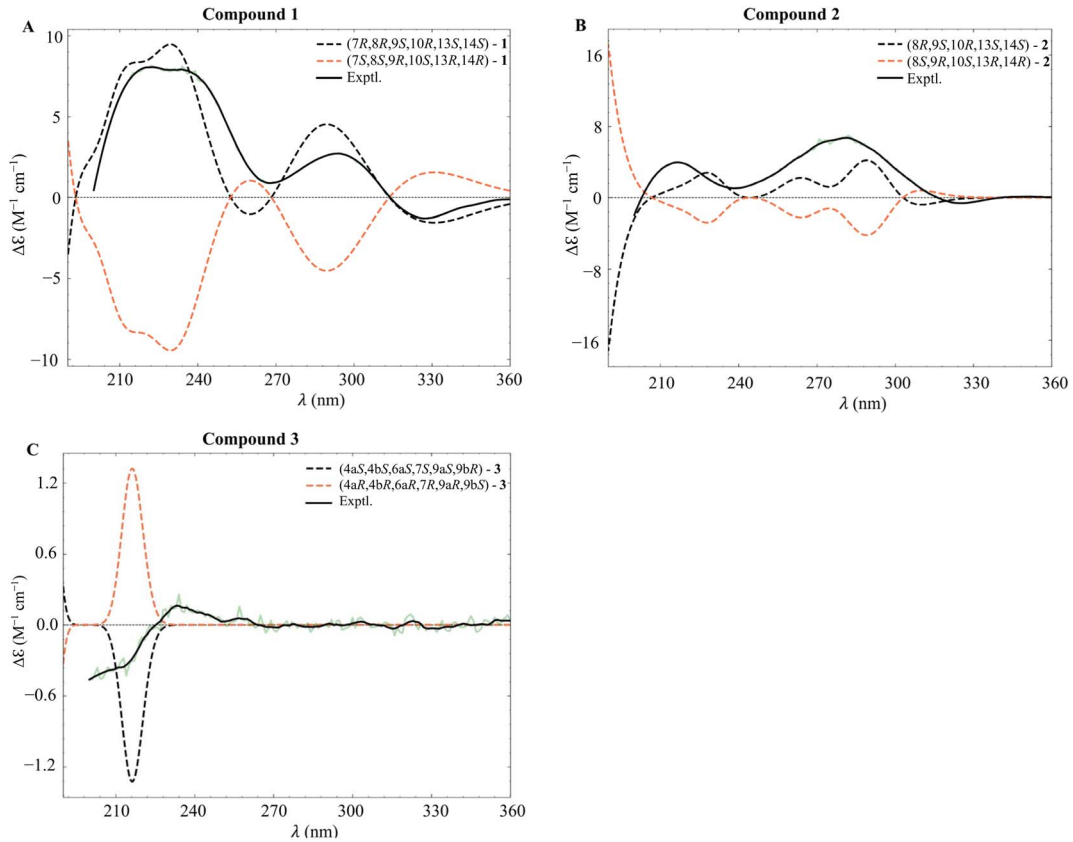


Fig. 4 Calculated (dotted black and orange lines) and experimental (solid black line) ECD spectra of (A) trestione (**1**), (B) formestane (**2**), and (C) oxandrolone (**3**) in MeOH.

values. Thus, the absolute configuration of compound **1** was determined as 7*R*,8*R*,9*S*,10*R*,13*S*,14*S*. The structure of compound **1** was identified as 7α-methylestr-4-ene-3,17-dione (mentabolan, also known as MENT dione, or trestione), a synthetic anabolic–androgenic steroid (AAS) and derivative of 19-nortestosterone. This represents the first report of its isolation from a natural source.

This compound has been clinically employed as a specialized androgen for male contraception, designed to preserve libido and muscle/bone health while potentially reducing prostate stimulation, a limitation of conventional testosterone therapy.[14,15]

4-Hydroxyandrost-4-ene-3,17-dione (**2**), trivially known as formestane, was isolated as a white powder. It was assigned the molecular formula $C_{19}H_{26}O_3$ based on its (+)-HRESI mass spectrum, which revealed a molecular ion peak $[M + H]^+$ (Fig. S12) at *m*/*z* 303.1952 (calcd for $C_{19}H_{27}O_3$, 303.1955), corresponding to seven DBE (double bond equivalents). Its IR spectrum showed strong absorption bands for the diosphenol (3381, 1663, and 1628 cm^{-1}), C–H (2968–2884 cm^{-1}), C=O (1736 cm^{-1}), and C_{sp^2}–O (1159 cm^{-1}) stretching vibrations (Fig. S13). The UV spectrum exhibited a characteristic absorption maximum at λ_{max} 277 nm (Fig. S14).

It is worth noting that the molecular ion, as shown by the ESI-MS (electrospray ionisation mass spectrometry), differed by 16 mass units from that of compound **1**. This suggests compound **2** has an additional hydroxyl group. The chemical structure of **2** was therefore deduced by comparison to that of compound **1**. The ^1H and ^{13}C NMR spectra of **2** (Fig. S15 and S16) exhibited similarities to those of **1**. Notably, analysis of the ^{13}C NMR spectrum in conjunction with the HSQC spectrum (Fig. S17) also revealed the presence of 19 carbon signals: (a) four sp^2 carbon signals in the downfield region, including two ketonic carbonyl carbons at δ_C 220.6 (C-17) and 193.4 (C-3), and

© 2026 The Author(s). Published by the Royal Society of Chemistry

two olefinic carbons at δ_C 141.3 (C-5) and 139.1 (C-4); and (b) fifteen sp^3 carbon signals in the range of δ_C 54.3–13.7 ppm. The main differences, as deduced from the ^1H NMR spectra of both compounds, were the signals of the following functional groups whose points of attachment in the structure of **2** were supported by HMBC correlations: (i) a hydroxyl group (δ_H 6.08) attached to C-4 as its proton showed cross-peaks with the carbon signals at δ_C 193.4 (C-3), 141.3 (C-5), 139.1 (C-4), 37.8 (C-10), and 31.7 (C-2); (ii) a methyl group ($\delta_{H/C}$ 1.18/17.1) was found to be attached to C-10 as its protons (H-19) correlated with the carbon signals of C-4, C-9 (δ_C 54.3), C-10 (δ_C 37.8), and C-1 (δ_C 34.6); and (iii) eight diastereotopic methylene signals were identified in the range of δ_H 3.04–1.05 for compound **2**. Those for H-6 (δ_H 3.04; 1.99) showed cross-peaks with the carbon signals of C-5 (δ_C 141.3), C-4 (δ_C 139.1), C-10 (δ_C 37.8), and C-8 (δ_C 34.7) (Fig. 2 and S18). In contrast, in compound **1**, seven such methylene signals were observed in the range of δ_H 2.49–1.24 ppm. The ^1H–^1H COSY spectrum (Fig. S19) confirmed the spin systems, including correlations between H-6 and H-7, and between H-8 and H-9. These data were consistent with previously reported findings for formestane,[16] a synthetic steroidal compound that suppresses the oestrogen production by inhibiting the aromatase enzyme that converts androgens into estrogens.[13]

The absolute configuration of **2** was established by ECD calculations performed for both enantiomers using the same protocol described above for compound **1**. The conformational search identified three conformers with Boltzmann populations of 94.95%, 5.04%, and 0.01%. Comparison of the Boltzmann-weighted spectrum (σ = 0.20 eV) revealed that the (8*R*,9*S*,10*R*,13*S*,14*S*) enantiomer well reproduced the experimental ECD profile. It particularly matched the sign, position, and relative intensity of the negative Cotton effect near 320 nm and the broader band centred around 280 nm (Fig. 4B and S21). The opposite enantiomer yielded the mirror-image spectrum, ruling out that configuration. Notably, the calculated optical rotation (+141.6) was opposite in sign to the experimental value (−78.1). Although this discrepancy is notable, it does not affect the configurational assignment, which was based primarily on ECD spectral comparison. Optical rotation is a single-value property that is highly sensitive to conformational averaging, solvent effects, and the choice of computational level.[17,18] In contrast, ECD provides a wavelength-dependent fingerprint with multiple diagnostic bands and is therefore inherently more reliable for absolute configuration determination.[19,20] The excellent agreement between the experimental and calculated ECD spectra for compound **2** supports the assigned (8*R*,9*S*,10*R*,13*S*,14*S*) configuration, consistent with the known configuration of formestane.

Possible contributing factors to the optical rotation discrepancy include: (i) incomplete conformational sampling, where high-energy conformers with large negative rotations may have been underrepresented or missed; (ii) limitations of the B3LYP-D3BJ/def2-TZVP level for accurate optical rotation prediction; (iii) neglect of explicit solute–solvent interactions and/or aggregation effects by the PCM model;[21] and (iv) minor experimental uncertainties in the specific rotation measurement. Nonetheless, the ECD-based assignment is considered robust. Future VCD (vibrational circular dichroism) or ROA (Raman optical activity) studies could provide independent confirmation.[22,23]

Formestane (4-hydroxyandrostenedione) (**2**) is an aromatase inhibitor which significantly reduces plasma levels of estrogen and has shown antitumour activity in postmenopausal women with breast cancer. It was formerly used to treat hormone-receptor-positive breast cancer in postmenopausal women, but has largely been replaced by cheaper, orally active medications.[24]

Oxandrolone (**3**) was isolated as a white powder. Positive-ion mode HRESIMS analysis established the molecular formula as $C_{19}H_{30}O_3$, based on the observed molecular ion peak $[M + H]^+$ at *m*/*z* 307.2266 (calcd for $C_{19}H_{31}O_3$, 307.2268) (Fig. S22), corresponding to five degrees of unsaturation. Its IR spectrum revealed characteristic vibrational modes, including hydroxyl stretching (3516 cm^{-1}), aliphatic C–H stretching (2976–2859 cm^{-1}), lactone carbonyl (1717 cm^{-1}), and C–O stretching (1036 cm^{-1}) (Fig. S23). The UV spectrum showed a pronounced absorption maximum at λ_{max} 201 nm (Fig. S24).

Analysis of the ^1H NMR spectrum of oxandrolone (**3**) (Fig. S25), together with its ^{13}C NMR (Fig. S26) and HSQC-DEPT (Fig. S27) spectra, revealed signals for: (a) three quaternary methyl groups at $\delta_{H/C}$ 1.17/26.2, 1.00/10.3, and 0.85/14.6; (b) eight sp^3 methylene (CH_2) groups, exhibiting sixteen diastereotopic protons. This includes a pair of geminal coupled protons at δ_H 4.25 and 4.00 (1H each, d, J = 10.7 Hz, δ_C 82.6), characteristic of an oxygenated CH_2 group. Another methylene, attached to a sp^2 carbon, appeared as two doublets of doublets at δ_H 2.49 and 2.23 (1H each, dd, J = 12.9, 6.0 Hz, δ_C 34.6). The remaining methylene signals were observed in the range of δ_H 1.83–0.95 ppm (δ_C 39.1–28.1 ppm); (c) four methines at $\delta_{H/C}$ 1.23/51.7, 0.89/50.8, 1.77/41.2, and 1.48/36.9; and (d) four quaternary carbons, including the lactone carbonyl at δ_C 173.8 and an oxygenated carbon at δ_C 82.2 as identified in the ^{13}C NMR spectrum (Fig. S26). These data are consistent with those reported for oxandrolone (also known as 17β-hydroxy-17α-methyl-2-oxa-5α-androstan-3-one) and related compounds, including 6α-, 9α-, 12β-, and 15α-hydroxy-oxandrolones.[25] The structure was further corroborated by key HMBC and ^1H–^1H COSY correlations. Notably, HMBC cross-peaks were observed between the methyl proton signal at δ_H 1.17 and the carbon resonances at δ_C 82.2 (C-17), 46.7 (C-13), and 39.1 (C-16); and between the proton signal at δ_H 0.85 with the carbon signals at δ_C 82.2 (C-17), 51.7 (C-14), 46.7 (C-13), and 32.5 (C-12), which enabled attaching these protons at C-17 and C-13, respectively. The methyl group (C-19) was attached to C-10, as evidenced by HMBC correlations between its proton signals at δ_H 1.00 and the carbon signals at δ_C 82.6 (C-1), 50.8 (C-9), 41.2 (C-5), and 35.9 (C-10). Further HMBC cross-peaks were observed between the geminal methylene protons at δ_H 4.25 and 4.00 (H-1) with the signals of C-3 (δ_C 173.8), C-9, C-5, and C-10; and between the CH_2 protons at δ_H 2.49 and 2.23 (H-4) with the carbon signals of C-6 (δ_C 28.1), C-5, and C-10 (Fig. 2). These CH_2 protons also displayed ^1H–^1H COSY correlations with the methine proton signal at δ_H 1.77, which in turn showed cross-peaks with the CH_2 protons at δ_H 1.45 and 1.23. Additionally, ^1H–^1H COSY correlations were observed between the methine proton at δ_H 1.26 (H-

© 2026 The Author(s). Published by the Royal Society of Chemistry

14) with both the methylene protons at δ_H 1.59 and 1.29 (H-15), as well as another methine at δ_H 1.48 (H-8) (Fig. 2 and S29).

The relative configurations of the chiral centres at C-8, C-9, C-10, C-13, and C-14 were assigned by analogy to compounds **1** and **2**. Key NOESY correlations supported the relative stereochemistry. A *cis*-relationship was indicated between the methine proton H-8 (δ_H 1.48) with both methyl protons H-18 (δ_H 0.85) and H-19 (δ_H 1.00). Furthermore, NOESY correlations between H-5 (δ_H 1.77) and H-9 (δ_H 0.89), and between H-14 (δ_H 1.23) and H-20 (δ_H 1.17), established their spatial proximities (Fig. S30 and 3). The complete ^{1}H and ^{13}C NMR data assignments for oxandrolone (**3**) are summarised in Table 1.

The absolute configuration of compound **3** was determined by comparing experimental and calculated ECD spectra for both enantiomers according to the same protocol described above. For this compound, the conformational analysis identified two conformers (populations: 65.04% and 34.96%), differing primarily in the orientation of the hydroxyl group. The calculated spectrum of the (4a*S*,4b*S*,6a*S*,7*S*,9a*S*,9b*R*) enantiomer (σ = 0.15 eV) was found to be consistent with the experimental data. It correctly replicated the negative Cotton effect near 210 nm despite the relatively high noise-to-signal ratio of the experimental spectrum (Fig. 4C and S31). The mirror-image spectrum obtained for the opposite enantiomer was clearly incompatible. Additionally, the predicted optical rotation (−40.5) was in reasonable agreement with the experimental value (−63.7), reinforcing the configurational assignment. Collectively, these results led to the assignment of the absolute configuration of compound **3** as 4a*S*,4b*S*,6a*S*,7*S*,9a*S*,9b*R*, which matches the known configuration of oxandrolone.

Oxandrolone is a synthetic anabolic–androgenic steroid (AAS) with weak androgenic activity and a high anabolic effect. First synthesized in 1962, it was introduced to the U.S. market in 1964 under the brand names of Anavar® and Oxandrin®. It has been used to treat alcoholic hepatitis, Turner syndrome, and osteoporosis.[18] It is the only U.S. FDA (Food and Drug Administration)-approved steroidal drug to promote weight gain after surgery, trauma, or chronic infection, and to relieve bone pain from osteoporosis.[26]

3,4-Dimethoxyacetophenone (**4**) was obtained as a white powder in CH_2Cl_2/MeOH (95 : 5), and its low-resolution EIMS (electron ionisation mass spectrum) displayed the $[M]^{\bullet+}$ peak at *m*/*z* 180. Analysis of its mass spectrum along with its 1D and 2D NMR spectra enabled us to assign the molecular formula $C_{10}H_{12}O_3$ to **4**, implying five double bond equivalents.

Its ^{1}H NMR spectrum exhibited proton signals at δ_H 7.56 (1H, dd, J = 8.3, 1.9 Hz), 7.51 (1H, d, J = 1.9 Hz), and 6.87 (1H, d, J = 8.3 Hz) characteristic of a 1,3,4-trisubstituted benzene ring system. In addition, signals for two methoxy protons were observed at δ_H 3.93 and 3.92. The signal of a deshielded 3-proton singlet was observed at δ_H 2.55 (Fig. S33 and Table 2). These data were similar to those previously reported for the natural acetophenone, apocynin.[27]

Analysis of its ^{13}C NMR and HSQC spectra (Fig. S34 and S35) revealed the presence of one carbonyl at δ_C 196.8; three aromatic methine carbons at δ_C 123.3, 110.1, 110.0; three aromatic quaternary carbons at δ_C 153.3, 149.1, and 130.5; two methoxy carbons at δ_C 56.3 and 56.2; and a methyl carbon at δ_C 26.3 (C-2) (Table 2). The methoxyl groups were located at positions 3′ and 4′ of the aromatic ring based on HMBC correlations observed between the protons at δ_H 3.93 and C-4′ (δ_C 153.3), and between the protons at δ_H 3.92 and C-3′ (δ_C 149.1). The acetyl group was located at 1′ of the aromatic ring on the basis of observed HMBC correlations between the methyl protons at δ_H 2.55 and carbon signals at δ_C 130.5 (C-1′), 123.3 (C-6′), and 196.8 (C=O) (Fig. S36 and 2). The ^{1}H–^{1}H COSY spectrum, in addition to the expected vicinal correlations (H-5′ and H-6′), exhibited weak but clear long-range correlations between the methoxy protons at δ_H 3.93 and H-5′ (δ_H 6.87), and between δ_H 3.92 and H-2′ (δ_H 7.51). This further confirmed the methoxyl groups assignment (Fig. S37 and 2).

Table 2 ^{1}H (400 MHz) and ^{13}C (100 MHz) NMR data of compound **4** in $CDCl_3$

No.	δ_H mult. (J in Hz)	δ_C, type
1	—	196.8, C
2	2.55 s	26.3, CH_3
1′	—	130.5, C
2′	7.51 d (1.9)	110.1, CH
3′	—	149.1, C
4′	—	153.3, C
5′	6.87 d (8.3)	110.0, CH
6′	7.56 dd (8.3, 1.9)	123.3, CH
3′-OCH_3	3.92 s	56.2, CH_3
4′-OCH_3	3.93 s	56.3, CH_3

The complete NMR data of compound **4** (Table 2) were consistent with those reported for 3,4-dimethoxyacetophenone,[28] an intermediate in the synthesis of papaverine, a clinically used vasodilator and antispasmodic agent.

Overall, the chemical investigation of the dung-derived *Penicillium tanzanicum* strain led to the isolation of three pharmaceutically established steroid drugs *viz*. trestione (**1**), formestane (**2**), and oxandrolone (**3**), alongside a naturally occurring acetophenone (**4**). Notably, **1** and **2** were further detected in the crude extract of the strain cultured under identical conditions (Fig. S38). It is worth noting that the isolation of compounds from natural sources previously regarded as synthetic is not unprecedented, as synthetic benzodiazepines and gamma-hydroxybutyrate have subsequently been reported to occur naturally.[29,30]

2.2. Plausible biogenic relationship between steroids

A speculative biosynthetic pathway for the isolated steroids (**1**–**3**) is proposed in Fig. 5, based solely on structural correlations. The sequence follows known fungal sterol transformations, beginning with the cyclization of squalene 2,3-epoxide to yield cholesterol. Side-chain cleavage of cholesterol could afford pregnenolone, which might be converted to progesterone through the action of 3β-HSD (3β-hydroxysteroid dehydrogenase). Progesterone is then hypothetically branched toward 17α-hydroxyprogesterone and androstenedione *via* oxidative modifications, including C-2β hydroxylation, methyl migration, and C-4 hydroxylation. It is worth noting that no genomic,

© 2026 The Author(s). Published by the Royal Society of Chemistry

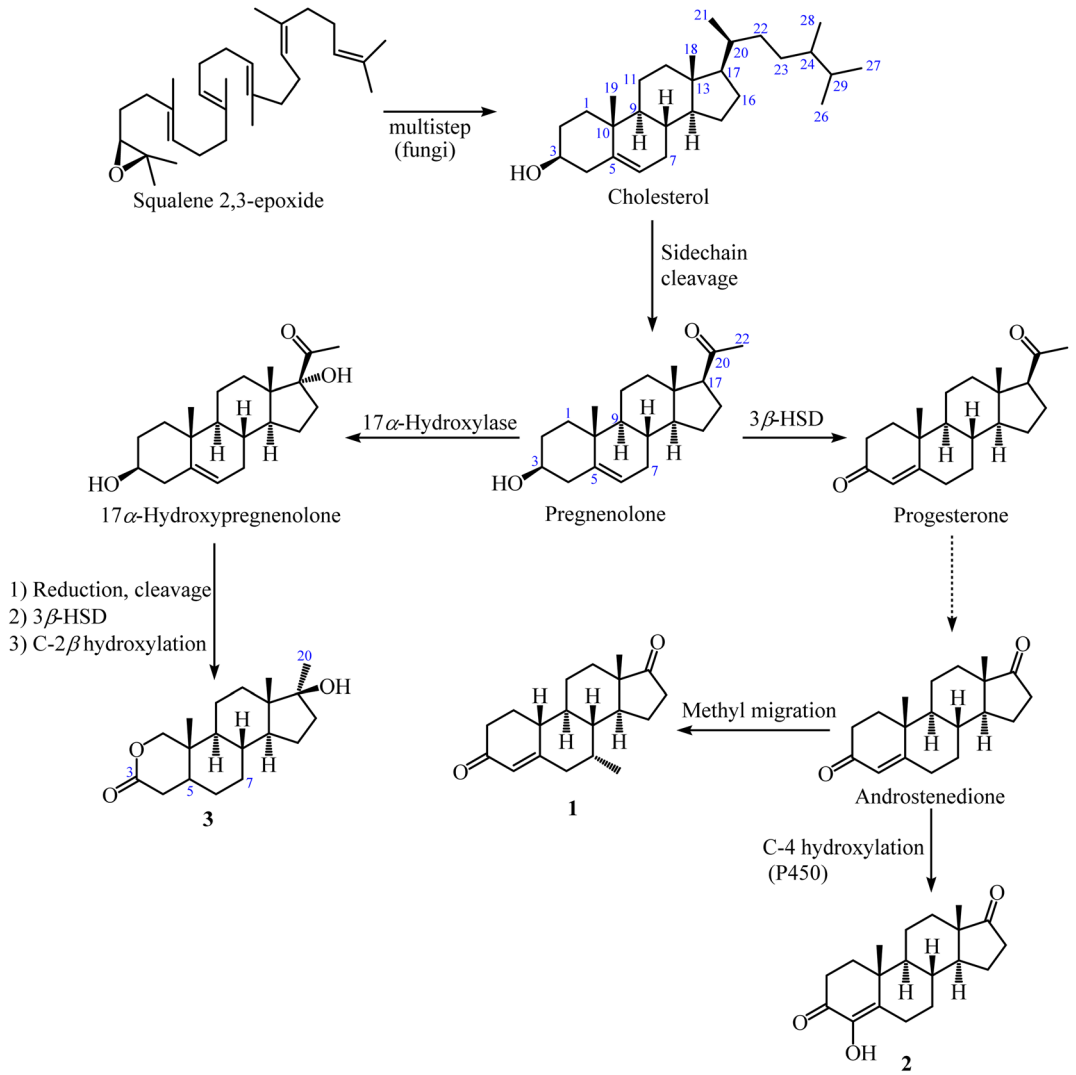


Fig. 5 Proposed biogenic relationship for steroids **1–3**. General background on fungal sterol metabolism can be found in the literature.[31,32]

enzymatic, or isotopic evidence is available in this study to support these specific transformations in this organism. The enzymatic assignments are inferential and should be treated as hypothetical. The scheme is presented as a working model, not as an established biogenetic route.[31,32]

The thirteen known compounds were characterised as integracide G (**5**),[33] anhydrofusarubin (**6**),[34] 5-hydroxydihydrofusarubin C (**7**),[35] anhydrojavanicin (**8**),[36] (+)-solaniol (**9**),[37] (1*S*,4*S*,10*S*)-6,9-dihydroxy-8-methoxy-10-(2-oxopropyl)-3,4-dihydro-1,4-methanobenzo[*c*]oxepin-5(1*H*)-one (**10**),[35] apocynin (**11**),[27] *p*-hydroxyacetophenone (**12**),[38] *p*-hydroxybenzaldehyde (**13**),[39] *N*-(2-phenylethyl)acetamide (**14**),[40] (4*R*,5*S*)-5-hydroxy-4-hexanolide (**15**),[41] 3′-*O*-acetylchloramphenicol (**16**),[42] and lignoren (**17**),[43] by comparing the observed and reported spectroscopic data.

2.3. Biological assays

With the aim of identifying potential lead compounds among the reported steroidal drug-like natural products, their antimicrobial, antiplasmodial activities, and haemolytic effects were evaluated alongside the antimicrobial activities of other isolates. Notably, several studies have highlighted the emerging anti-infective potential of steroids, with demonstrated antimicrobial and antiplasmodial properties.[44–46]

2.3.1. Antimicrobial activity. The antimicrobial activity of the crude extract and the isolates (**1–16**) was evaluated using the broth microdilution method to determine their minimum inhibitory concentrations (MICs) (Table 3). The panel of test organisms included one mycobacterium (*Mycobacterium tuberculosis*), ESKAPE pathogens (*Enterococcus faecium*, *Staphylococcus aureus*, *Klebsiella pneumoniae*, *Acinetobacter baumannii*, *Pseudomonas aeruginosa*, and *Enterobacter* species), and one fungus (*Candida albicans*).[47]

The crude extract exhibited moderate activity against *M. tuberculosis* H37Rv (MIC = 400 μg mL^{-1}) and significant activity against *E. faecalis* ATCC 29212 and *E. faecium* ATCC 35667 (MIC = 50 μg mL^{-1}). According to the threshold defined by Tamokou *et al.* (2017),[48] compound **13** showed moderate activity against *M. tuberculosis* H37Rv and *S. aureus* ATCC 29213 (MIC = 50 μg mL^{-1}), and weak activity against *S. aureus* ATCC 29213 (MIC =

© 2026 The Author(s). Published by the Royal Society of Chemistry

Table 3 Antimicrobial activity (MIC, μg mL^{-1}) of crude extract and compounds **1–16** [a]

Bacterial/fungal strain	**1–7, 10, 11, 14–16**	**8**	**9**	**12**	**13**	Crude extract	[#]Mfx	[#]RMP	[#]AmB
M. tuberculosis H37Rv	>100	—	>100	>100	50	400	—	0.32	—
S. aureus ATCC 29213	>100	—	100	—	50	>400	<0.10	—	—
S. aureus ATCC 700699	>100	>100	>100	—	100	—	1.56	—	—
E. faecalis ATCC 29212	>100	>100	>100	—	>100	50	<0.78	—	—
E. faecium ATCC 35667	>100	50	50	—	>100	50	3.12	—	—
E. coli ATCC 25922	>100	—	>100	—	>100	>400	—	6.25	—
P. aeruginosa ATCC 27853	>100	—	>100	—	>100	>400	—	25	—
A. baumannii BAA-747	>100	—	>100	—	>100	>400	—	1.56	—
C. albicans ATCC 24433	>100	>100	>100	>100	>100	>400	—	—	0.78

[a] MIC = minimum inhibitory concentration; — = not tested; serial dilution ranges: 100–0.78 μg mL^{-1} for test compounds and 400–3.125 μg mL^{-1} for the crude extract; [#]reference drugs: Mfx = moxifloxacin, RMP = rifampicin, AmB = amphotericin B.

100 μg mL^{-1}). In addition, **8** displayed moderate activity against *E. faecium* ATCC 35667 (MIC = 50 μg mL^{-1}). Compound **9** also demonstrated moderate activity against *E. faecium* ATCC 35667 (MIC = 50 μg mL^{-1}) and weak activity against *S. aureus* ATCC 29213 (MIC = 100 μg mL^{-1}), while compound **11** exhibited only weak activity against *E. faecalis* ATCC 29212 (MIC = 100 μg mL^{-1}).

2.3.2. Antiplasmodial efficacy. Compounds **1–3** were evaluated *in vitro* for their antiplasmodial potency against the multi-resistant *Plasmodium falciparum* (*Pf*Dd2) strain (Table 4). Activity was classified according to the criteria established by Batista and collaborators (2009).[49] Trestione (**1**) and formestane (**2**) exhibited good antiplasmodial activity, with IC_{50} values of 26.58 and 15.03 μM, respectively. The dose–response curves for both compounds are presented in Fig. 6, showing a clear concentration-dependent inhibition of parasite growth. These findings are consistent with those of Douanla and co-workers (2015),[50] who reported potent antiplasmodial activity of ergostane steroids. The comparatively stronger activity of compound **2** may be attributed to the presence of a hydroxyl group, which can enhance hydrogen bonding with parasite targets and improve molecular recognition within the binding pocket.[51] Collectively, these results suggest that such compounds may represent promising candidates for further investigation as antiplasmodial agents.

Table 4 Antiplasmodial efficacy against the multi-resistant (*Pf*Dd2) strain of *Plasmodium falciparum* and haemolysis activity on normal erythrocytes (%) of compounds **1–3** [a]

Compounds	IC_{50} value (μM) ± SD	% Haemolysis ± SD (conc. = 250 μg mL^{-1})
1	26.58 ± 2.15	0.63 ± 0.28
2	15.03 ± 0.14	0.88 ± 0.21
3	n.a	0.86 ± 0.16
DHA	0.0058 ± 7.15 × 10^{-5}	—
ART	0.020 ± 6.5 × 10^{-5}	—
CQ	0.86 ± 0.0453	—

[a] IC_{50}: inhibitory concentration 50; n.a: not active; SD: standard deviation; DHA: dihydroartemisinin; ART: artemisinin; CQ: chloroquine; conc.: concentration.

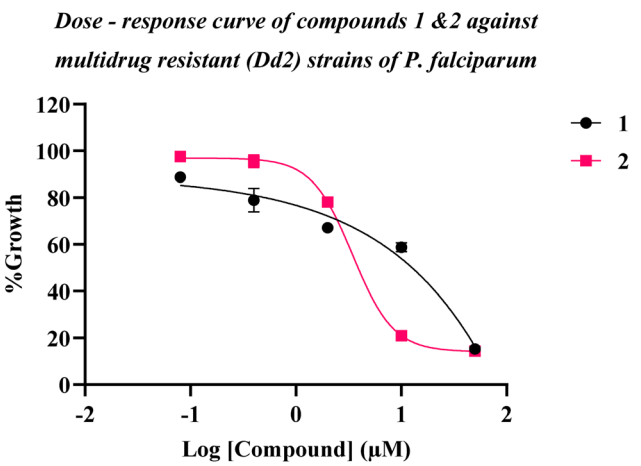


Fig. 6 Dose–response curves of compounds **1** and **2** on *Pf*Dd2.

2.3.3. Haemolytic activity on normal erythrocytes. Compounds **1–3** induced minimal haemolysis (<2%) following 3 h treatment of fresh erythrocytes across a concentration range of 250 to 15.63 μg mL^{-1} (Table 4), when compared to the standard control Triton X-100 (100% haemolysis). Irrespective of the concentration tested, the compounds exhibited negligible haemolytic effects and did not cause adverse events on erythrocytes at drug concentrations effective against the parasite. These findings suggest that the observed antimalarial activity of these steroids is primarily not attributable to erythrocyte lysis, thereby supporting their potential as safe antiplasmodial agents.

3. Experimental

3.1. General experimental procedures

Silica gel-coated cards (0.25 mm thick, E. Merck, Germany) were used for TLC (thin layer chromatography) analyses. Flash silica gel (E. Merck, Germany 40–63 μm, 230–400 mesh) was used in column chromatography (CC) for initial fractionation. Final purification of compounds was carried out using silica gel (E. Merck, Germany 15–40 μm, 230–400 mesh) columns. Infrared (IR) spectra (cm^{-1}) were recorded on a Shimadzu IRAffinity-1

© 2026 The Author(s). Published by the Royal Society of Chemistry

spectrophotometer equipped with a PIKE MIRacle ATR-Reflector (diamond crystal plate). The spectra were acquired in the solid state using the attenuated total reflection (ATR) technique over the 4000–600 cm^{-1} region with a spectral resolution of 4 cm^{-1} (25 scans). Ultraviolet (UV) spectra were recorded on a Hitachi Spectrophotometer U-5100 in methanol using a Hellma Analytics quartz cuvette (spectral range 200–2500 nm). Optical rotations were measured on a Jasco P-2000 polarimeter in methanol at 20 °C (c = 0.1%); the specific optical rotation was the mean of 30 measurements, calculated by the device for a 10 cm path length.

High-resolution electrospray ionisation mass spectrometry (HRESIMS) spectra were recorded with an Agilent 1290 Infinity III UHPLC system (column 50 × 2.1 mm, 2 μm, C18 Ascentis Express; solvent A: H_2O + 0.1% formic acid; solvent B: MeCN + 0.1% formic acid; gradient: 10% B increasing to 98% B in 8 min and then maintaining 98% B for 1 min; flow rate 0.4 mL min^{-1}; UV-vis detection 200–600 nm) connected to a Bruker Daltonics timsTOF Pro 2 ESI-TOF mass spectrometer (scan range 100–2500 m/z). Electron impact mass spectra (EI-MS) were performed on a JEOL Single-Quadrupole-MS JMS-Q1600GC, while high-resolution electron impact mass spectra (HREI-MS) were recorded on a JEOL JMS HX-110.

Nuclear magnetic resonance (NMR) experiments were recorded on 600 and 500 MHz for ^{1}H NMR, 150 and 125 MHz NMR spectrometers for ^{13}C NMR, while two-dimensional NMR experiments were recorded on Bruker Avance 600 and 500 spectrometers. All NMR experiments were performed in deuterated chloroform or methanol. The ^{1}H and ^{13}C NMR chemical shifts (δ) are reported in ppm, and coupling constants (J) are measured in Hz.

3.2. Fungal material

The fungus was isolated using the moist chamber method.[52] Partially decomposed bull dung was collected at Ecopark in Yaounde (Centre Region of Cameroon). The dung was rehydrated in deionized H_2O supplemented with chloramphenicol and incubated in deep-dish Petri plates lined with filter paper to simulate natural dung decomposition. The Petri plates were examined periodically with a stereomicroscope for fungal growth. The strain of *P. tanzanicum* was isolated by germinating mycelium on malt extract agar amended with chloramphenicol and identified by Inqaba Biotec (https://inqababiotec.co.za/), through ITS nrDNA sequencing (Table S4). A voucher specimen of this strain is stored at −80 °C in our laboratory under the number CECA077.

For identification, genomic DNA was extracted using the Quick-DNA™ Fungal/Bacterial kit (Zymo Research, Catalogue no. D6005). The ITS target region was amplified with OneTaq® Quick-Load® 2X Master Mix (NEB, Catalogue no. M0486) using ITS-1 and ITS-4 primers. The PCR product was analysed by gel electrophoresis and cleaned up enzymatically using the EXOSAP method. The extracted fragments were sequenced in both the forward and reverse directions (Nimagen, BrilliantDye™ Terminator Cycle Sequencing Kit V3.1, BRD3-100/1000) and subsequently purified (Zymo Research, ZR-96 DNA Sequencing Clean-up Kit™, Catalogue no. D4050). The purified fragments were analysed on the ABI 3500xl Genetic Analyser (Applied Biosystems, ThermoFisher Scientific). The resulting sequence data (*.ab1 files) were processed using DNASTAR software and identified through a BLAST search (NCBI).

3.3. Fermentation and extraction

A large-scale culture of *P. tanzanicum* mycelia was carried out in solid media using the method reported by Mountessou *et al.* (2023)[53] with some modifications. A total of 60 flasks (1 L each) containing 110 g rice and 110 mL water were autoclaved at 121 °C for 20 min. Each flask received about six small pieces of mycelium from an MEA plate under sterile conditions. After 15 days of growth at 27 °C, the culture media were extracted with EtOAc, yielding 83.0 g of crude extract.

3.4. Isolation

A portion of the EtOAc extract (80.0 g) was subjected to column chromatography over silica gel (70–230 mesh) using a stepwise gradient of ethyl acetate in *n*-hexane, followed by EtOAc. A total of 25 fractions, each approximately 500 mL were obtained and combined based on TLC profiles into five main fractions ($Fr._{1–5}$).

Fraction $Fr._2$ (10.5 g, *n*-Hex/EtOAc 80 : 20 and 70 : 30) was subjected to column chromatography over silica gel (70–230 mesh) and eluted with an isocratic mixture of CH_2Cl_2/MeOH (98 : 2) to give compounds **1** (230 mg, 0.29%), **3** (23 mg, 0.029%), and **5** (2 mg, 0.0025%) and a mixture of **16** and **2**. The mixture was further purified over Sephadex LH-20 (CH_2Cl_2/MeOH 50 : 50), affording **16** (1.9 mg, 0.0024%) and **2** (33 mg, 0.041%). Further purification of the intermediate fractions from this column yielded **14** (4 mg, 0.005%).

Fraction $Fr._3$ (3.0 g, *n*-Hex/EtOAc 60 : 40) was chromatographed on silica gel and eluted with an isocratic mixture of CH_2Cl_2/MeOH (95 : 5) to give compounds **4** (1.0 mg, 0.0013%), **11** (1.6 mg, 0.0020%), **12** (1.0 mg, 0.0013%), and **13** (1.5 mg, 0.0019%).

Fraction $Fr._4$ (2.6 g, *n*-Hex/EtOAc 50 : 50) was fractionated on silica gel and eluted with an isocratic mixture of CH_2Cl_2/MeOH (90 : 10) to give eight subfractions which were further purified by normal-phase HPLC (250 × 10 mm, 5 μm particle size, flow rate 4 mL min^{-1}) with CH_2Cl_2/MeOH (90 : 10) to yield **10** (1.5 mg, 0.0019%), **7** (1.1 mg, 0.0014%), **6** (1.4 mg, 0.0018%), **9** (3.0 mg, 0.0038%), **8** (1.5 mg, 0.0019%), and **15** (4.0 mg, 0.0050%).

Fraction $Fr._5$ (1.8 g, *n*-Hex/EtOAc 40 : 60) was purified on silica gel and eluted with an isocratic mixture of CH_2Cl_2/MeOH (80 : 20) to yield **17** (1.0 mg, 0.0013%).

3.5. Calculation of ECD spectra

ECD spectra were calculated for compounds **1–3**. The conformational search was carried out using the CREST program package[54,55] with a temperature of 300 K and an energy window of 6 kcal mol^{-1}. For compounds **1** and **3**, two conformers were identified, whereas three conformers were found for compound **2**. The resulting conformers were subsequently optimised at the DFT level employing the B3LYP-D3BJ functional in combination

© 2026 The Author(s). Published by the Royal Society of Chemistry

with the def2-TZVP basis set[56–58] as implemented in the Gaussian 16 program package.[59] To verify that the identified stationary points were true minima, vibrational frequencies were computed at the same level of theory; all frequencies were positive, enabling us to estimate Boltzmann populations of the conformers using Gibbs free energies (ΔG) calculated at 298 K. Solvent effects were included through the Polarizable Continuum Model (PCM) using methanol as the solvent.[21]

For each geometry-optimised conformer, optical rotations were calculated at the wavelength of the sodium D-line (589.3 nm), as well as ECD spectra through time-dependent density functional theory (TDDFT) calculations (considering 16 electronic excitations), using the same aforementioned functional and basis set combination. Both length and velocity formalisms showed comparable results for rotatory strengths R for all transitions, and all spectra were reported using the length formalism. ECD spectra were generated using a home-made Python script that applies a Gaussian line-broadening function to the calculated rotatory strengths. Different σ values used to match the experimental spectra were 0.30, 0.20, and 0.15 eV (ref. 60) for compounds **1**, **2**, and **3**, respectively. Experimental spectra were smoothed prior to analysis using a second-order Savitzky–Golay filter[61] with a 15-point window and subsequently compared with the calculated spectra.

3.6. Physico-chemical properties of compounds 1–3

Trestione (**1**): white powder; $[\alpha]_D^{20}$ + 66.8 (*c* 0.1, MeOH) (calcd +97.1); UV (MeOH) λ_{max} (log ε) 241 (4.4521) 300 (2.3021) nm; (+)-HRESIMS *m*/*z* 287.2004 $[M + H]^+$ (calcd for $C_{19}H_{27}O_2$, 287.2006); IR (ATR) ν_{max} 1735, 1660, 1616, 1449, 1387, 1250, 1040, 1009, 878 cm^{-1}; ^1H and ^{13}C NMR data ($CDCl_3$, 600 MHz and 150 MHz) see Table 1.

Formestane (**2**): white powder; $[\alpha]_D^{20}$ −78.1 (*c* 0.1, MeOH) (calcd +141.6); UV (MeOH) λ_{max} (log ε) 277 (4.0816) nm; (+)-HRESIMS *m*/*z* 303.1952 $[M + H]^+$ (calcd for $C_{19}H_{27}O_3$, 303.1955); IR (ATR) ν_{max} 3404, 3381 (OH), 2945, 2928, 1736, 1663, 1628, 1404, 1381, 1354, 1238, 1213, 1159, 1098, 2024 cm^{-1}; ^1H and ^{13}C NMR data ($CDCl_3$, 600 MHz and 150 MHz) see Table 1.

Oxandrolone (**3**): white powder; $[\alpha]_D^{25}$ −63.7 (*c* 0.1, MeOH) (calcd −40.5); UV (MeOH) λ_{max} (log ε) 201 (3.0166) nm; (+)-HRESIMS *m*/*z* 307.2266 $[M + H]^+$ (calcd for $C_{19}H_{31}O_2$, 307.2268); IR (ATR) ν_{max} 3516, 2936, 2918, 1717, 1406, 1366, 1223, 1204, 1036, 1028, 932 cm^{-1}; ^1H and ^{13}C NMR data (CD_3OD, 600 MHz and 150 MHz) see Table 1.

3,4-Dimethoxyacetophenone (**4**): white powder; EI-MS *m*/*z* (rel. int., %): 180 (44), 165 (100), 150 (18), 137 (40), 122 (14), 83 (57); ^1H and ^{13}C NMR data ($CDCl_3$, 400 MHz and 100 MHz) see Table 2.

3.7. Biological assays

3.7.1. Antimicrobial assay

3.7.1.1. Media and strains. Single colonies obtained from agar plates of Gram-positive bacteria *Staphylococcus aureus* ATCC 29213, Methicillin-resistant/Vancomycin-intermediate *S. aureus* (MRSA/VISA) ATCC 700699, *Enterococcus faecalis* ATCC 29212, and *E. faecium* ATCC 35667, and Gram-negative bacteria *Escherichia coli* ATCC 25922, *Pseudomonas aeruginosa* ATCC 27853 and *Acinetobacter baumannii* BAA-747 were grown in Mueller–Hinton Broth (MHB, BD Difco, USA) and the yeast *Candida albicans* ATCC 24433 in YPD medium (1% yeast extract, 2% peptone, and 2% dextrose). The cultures were incubated at 37 °C and shaken at 180 rpm.

Mycobacterium tuberculosis H37Rv was grown in 7H9 medium supplemented with 10% ADS (0.85% NaCl, 5% BSA, 2% dextrose), 0.5% glycerol, and 0.05% tyloxapol at 37 °C at 80 rpm.

3.7.1.2. Minimum inhibitory concentrations (MICs) determination. MICs were determined using the broth microdilution method. The compounds and crude extract were dissolved in dimethyl sulfoxide (DMSO) and diluted in a 96-well plate in 50 μL of the respective medium in a 1 : 1 serial dilution, resulting in a final concentration ranging from 100 μg mL^{-1} to 0.78 μg mL^{-1} for the compounds and from 400 μg mL^{-1} to 3.125 μg mL^{-1} for the crude extract. Fifty microlitres of adjusted cell suspension (10^6 CFU per mL for all bacteria, 5×10^3 CFU per mL for *C. albicans*) were added to each well. Plates were incubated statically at 37 °C for 20–24 h (ESKAPE bacteria and yeast), or for 5 days at 37 °C and 5% CO_2 in a humidified atmosphere for *M. tuberculosis*. Readout was performed macroscopically for bacteria and *C. albicans*, whereas MIC is defined as the lowest concentration at which no visible growth appears in comparison to the controls. For *M. tuberculosis*, the resazurin reduction assay was utilized. Briefly, 10 μL of a 100 μg mL^{-1} resazurin solution was added to each well and re-suspended carefully. After 24 hours at room temperature, cells were fixed by adding 100 μL of a 10% formalin solution to each well. Fluorescence was measured at 535 nm excitation and 590 nm emission in a TECAN plate reader.

Moxifloxacin was used as a positive control for Gram-positive bacteria, rifampicin was used as a positive control for Gram-negative bacteria and *M. tuberculosis*, and amphotericin B was used as a positive control for *C. albicans*, while DMSO was used for all organisms as a solvent control.

Depending on the available quantity, the compounds were screened either as a single sample or in duplicate. For those exhibiting activity, the assay was subsequently repeated in triplicate to ensure reproducibility.

3.7.2. Antiplasmodial assay

3.7.2.1. Preparation of the drug master plate. Compounds **1**–**3** were dissolved in 100% DMSO (Sigma-Aldrich, Munich, Germany) at 10 mg mL^{-1}. Afterwards, master plates were prepared by mixing 10 μL of sample solutions with 190 μl of fresh RPMI 1640 incomplete (without HEPES, Albumax I, hypoxanthine and gentamicin) culture medium into a 96-well plate to yield a concentration of 500 μg mL^{-1} (5% DMSO) followed by a five-fold serial dilution. For each inhibitor, the intermediate concentrations ranged from 0.8 to 500 μg mL^{-1}. Chloroquine, Artemisinin and Dihidroartemisinin (Sigma-Aldrich, Munich, Germany), which were used as standard drugs, were prepared at 10 mM in sterile distilled water for chloroquine and 100% DMSO for artemisinin and dihydroartemisinin and serially diluted in an incomplete RPMI1640 medium. The master plates

© 2026 The Author(s). Published by the Royal Society of Chemistry

were frozen at −80 °C until use or freshly made the day of the assay.

3.7.2.2. Plasmodium falciparum growth inhibition assay

3.7.2.2.1. Maintenance of P. falciparum asexual-blood stages. The multi-resistant (*Pf*Dd2) (resistant to chloroquine, pyrimethamine, and mefloquine) *P. falciparum* strain obtained from BEI resources (https://www.beiresources.org/) was cultured and maintained in the presence of O positive human erythrocytes as previously described.[62] The cryotube containing the strain was pre-warmed to 37 °C for 2 min to facilitate thawing and the content was transferred to a 50 mL Falcon tube into which 100 µL of NaCl solution (12%) was added dropwise. After a 5 min rest, 5 mL NaCl solution (1.6%) was added dropwise to this mixture. The mixture was centrifuged at 2500 rpm for 5 min and the supernatant was removed. The pellet was washed once with complete RPMI 1640 [16.2 g L^{-1} RPMI 1640 (Sigma-Aldrich) containing 25 mM HEPES (Gibco, UK), 11.1014 mM glucose, 0.2% sodium bicarbonate (Sigma-Aldrich), 0.5% Albumax II (Gibco, USA), 1× hypoxanthine (Sigma, USA) and 4 µM Gentamicin (Sigma-Aldrich)]. The remaining pellet was maintained in fresh human group O positive erythrocytes suspended at 4% hematocrit in a complete RPMI 1640 culture medium. The suspension was placed in a 60 mm Petri dish and incubated at 37 °C in a humidified atmosphere containing 5% CO_2. The culture medium was renewed daily with a fresh complete medium to ensure optimal and continuous parasite growth. Blood smears were prepared and stained with 10% Giemsa solution, then observed under a light microscope (Huma Scope Classic) at 100× with oil immersion to check the conditions of the culture and parasite proliferation.

3.7.2.2.2. Synchronization of P. falciparum cultures. Prior to the antiplasmodial activity assessment, parasitic culture containing mainly the ring stage was synchronized 48 h beforehand. Synchronization consists of the selective destruction of advanced stages (trophozoite and schizont) of parasite development by treatment with 5% (*w*/*v*) D-sorbitol.[63] The erythrocyte membrane is normally impermeable to sorbitol, but parasite-induced channels in the membrane of infected cells allow sorbitol to pass through. When late-stage parasitized erythrocytes are suspended in a sorbitol solution, there is a net uptake of sorbitol and water into the erythrocytes, leading to swelling and hemolysis of these cells.[64] Experimentally, parasitic cultures containing at least 80% of the ring stage were centrifuged at 2500 rpm for 5 min, and the supernatant was removed and replaced with 5 mL of 5% (*w*/*v*) sorbitol solution. The mixture was thoroughly homogenized and incubated at 37 °C for 10 min, then centrifuged again at 2500 rpm for 5 min, followed by 3 rounds of washing with incomplete RPMI 1640 medium. After synchronization, the parasites were re-cultured in a complete RPMI 1640 medium at 4% hematocrit for the antiplasmodial experiments.

3.7.2.2.3. Inhibition of P. falciparum asexual blood stages. The antiplasmodial activity of the compounds (**1–3**) was assessed in 96-well flat-bottomed microplates (Sigma-Aldrich) according to the protocol described by Smilkstein *et al.* (2004),[65] based on the ability of parasites to multiply and survive in the presence of a defined concentration of the compound or reference molecule. Parasite growth was determined using SYBR Green I (Sigma-Aldrich), which binds to double-stranded DNA, producing a strong fluorescence with intensity proportional to the number of parasites present in the medium. Briefly, 90 µL of ring-synchronized parasite suspension prepared at 2% parasitemia and 1% hematocrit was incubated with 10 µL of compound at different pre-diluted concentrations. The positive control consisted of the reference molecules (dihydroartemisinin, artemisinin and chloroquine), while the negative control (100% growth) consisted of 100 µL of the parasite suspension. Plates were incubated for 72 h at 37 °C in a humidified incubator with 5% CO_2. Final concentrations in the test plates ranged from 50 µg mL^{-1} to 0.08 µg mL^{-1} (DMSO ≤0.5%) for compounds and from 1 µM to 0.0016 µM for dihydroartemisinin, artemisinin and chloroquine in a final volume of 100 µL. At the end of the incubation period, 100 µL of SYBR Green I lysis buffer (0.2 µL SYBR Green I/mL lysis buffer) consisting of Tris (20 mM; pH 7.5), EDTA (5 mM), saponin (0.008%, *w*/*v*), and Triton X-100 (0.08%, *v*/*v*) were gently added to each well, followed by a further 1 h incubation in the dark.[65] Fluorescence was then measured using a microplate reader (Infinite M200, Tecan) at excitation and emission wavelengths of 485 nm and 538 nm, respectively. Tests were performed in triplicate. The fluorescence values obtained were used to calculate inhibition percentages (% INH) using Microsoft Excel software, according to the formula:

$$\%\ \mathrm{INH} = 100 \times \frac{\text{fluorescence negative control} - \text{fluorescence test}}{\text{fluorescence negative control}}$$

Using GraphPad 8.0 software, median inhibitory concentrations (IC_{50}) were determined from sigmoidal concentration-response curves obtained by plotting the percentage of inhibition against the decimal logarithm of inhibitor concentration. The experiments were conducted in duplicate for three independent experiments, and the IC_{50} was expressed as mean ± SD.

3.7.3. Hemolysis assay. A haemolysis assay was performed as previously described,[66] against normal O^+ human red blood cells to assess the haemolytic effect of the test compounds at concentrations ranging from 250 to 15.63 µg mL^{-1}. Briefly, 100 µL of O^+ human red blood cells at 2% haematocrit were mixed with 100 µL of the test sample at a concentration ranging from 250 to 15.625 µg mL^{-1} in a 96-well plate, followed by incubation for 2 h at 37 °C. Triton X-100 0.5% (*v*/*v*) and fresh RPMI 1640 incomplete (without HEPES, Albumax I, hypoxanthine and gentamicin) culture medium, which induced 100% and 0% haemolysis in RBCs, were used as positive and negative controls, respectively. After 3 h of incubation at 37 °C, the preparation composed of lysed red blood cells and free haemoglobin was centrifuged at 1500 rpm for 5 min, and the supernatant was separated. Next, the amount of haemoglobin

© 2026 The Author(s). Published by the Royal Society of Chemistry

released in each supernatant was quantified spectrophotometrically at 540 nm using a microtiter plate reader (TECAN Infinite M200, USA) and compared to the negative control. The haemolysis percentage was calculated as follows:

$$\%\ \text{Haemolysis} = \frac{\text{absorbance of sample 540 nm} - \text{absorbance of blank sample 540 nm}}{\text{absorbance of positive control 540 nm}} \times 100$$

4. Conclusions

This study reports the first natural isolation of three pharmaceutically established steroidal drugs, trestione (**1**), formestane (**2**), and oxandrolone (**3**), together with fourteen additional metabolites from *Penicillium tanzanicum*. The discovery of these steroids from a natural source underscores the continued potential of the *Penicillium* genus as a prolific reservoir of bioactive compounds. Although the isolated steroids did not exhibit notable antimicrobial activity against the tested strains, compounds **1** and **2** demonstrated significant antiplasmodial activity against the multi-resistant *Plasmodium falciparum* (*Pf*Dd2) strain and low haemolysis activity on human erythrocytes, highlighting their promise as lead compounds warranting further investigation for antiplasmodial agents. In addition, the antimicrobial activities observed in the crude extract and selected isolates against *Mycobacterium tuberculosis*, *Staphylococcus aureus*, *Enterococcus faecalis*, and *E. faecium* reinforce the value of this fungal resource in the search for new antimicrobial leads. Collectively, these findings enrich the chemical profile of *P. tanzanicum* and validate the strategy of investigating fungi from underexplored ecological niches for drug discovery. Future work should focus on elucidating the biosynthetic pathways of compounds **1–3** and conducting in-depth biological assays to further characterize their activities.

Author contributions

J. T., and T. Y. D. Y.: isolation and purification of the fungus, fermentation, extraction, isolation, and structural elucidation of compounds. B. Y. G. M., A. T., L. V. G., and S. V.: data curation, and preparing the original data manuscript. A. T., L. V. G., K. J. N. T., M. B. T. T.: biological assays. J. T., A. A., R. K., and S. F. K.: reviewing, editing, and correcting the draft. J. T., B. Y. G. M., S. V., D. P., and S. F. K.: conceptualization and methodology. R. K., and S. F. K.: supervision, funding acquisition. All authors have read and agreed to the published version of the manuscript.

Conflicts of interest

The authors declare no conflict interest.

Data availability

The data generated and analysed during this study are available from the corresponding author upon reasonable request. Data related to the chemical structures and spectroscopic analysis of the isolated compounds are available in the supplementary information (SI). Supplementary information is available. See DOI: https://doi.org/10.1039/d6ra06849a.

Acknowledgements

This research was conducted within the framework of the Humboldt Research Hub-CECANAPROF project (3.4-CMR-Hub), funded by the Alexander von Humboldt (AvH) Foundation, which focuses on the investigation of antimicrobial natural products. The authors gratefully acknowledge the support of The World Academy of Sciences (TWAS) and the German Research Foundation (DFG). J. T. received funding through the TWAS-DFG Cooperative Visit Program for researchers from sub-Saharan Africa, while B. Y. G. M. and T. Y. Y. D. were supported by TWAS-ICCBS postdoctoral and postgraduate fellowships, respectively. The authors thank the CeMSA@HHU (Centre for Molecular and Structural Analytics @ Heinrich Heine University) for recording the mass-spectrometric data.

References

1 S. Singh and R. Khajuria, in *New and Future Developments in Microbial Biotechnology and Bioengineering*, Elsevier, 2018, pp. 201–215.
2 X.-C. Wang, Z.-K. Zhang and W.-Y. Zhuang, *J. Fungi*, 2023, **9**, 1150.
3 C. A. Lindsay, A. D. Kinghorn and H. L. Rakotondraibe, *Phytochemistry*, 2023, **209**, 113638.
4 G.-B. Ge, D.-C. Dai, X.-M. Zhou, W.-J. Wu, C.-J. Zheng, X.-M. Song and Y.-P. Luo, *Fitoterapia*, 2022, **157**, 105119.
5 M. Pangging, T. T. T. Nguyen and H. B. Lee, *Mycobiology*, 2021, **49**, 363–375.
6 C. M. Visagie, J. B. Renaud, K. M. N. Burgess, D. W. Malloch, D. Clark, L. Ketch, M. Urb, G. Louis-Seize, R. Assabgui, M. W. Sumarah and K. A. Seifert, *Persoonia*, 2016, **36**, 247–280.
7 B. Y. G. Mountessou, G. L. M. Tiani, J. Tchamgoue, R. Maharjan, A. Trucksess, R. Kalscheuer, M. I. Choudhary and S. F. Kouam, *Phytochem. Lett.*, 2026, **71**, 104095.
8 A. B. F. Kapche, P. Eckhardt, J. Tchamgoue, B. Tsakem, J. R. N. Kuete, A. Trucksess, A.-L. Njouonkou, B. K. Ponou,

© 2026 The Author(s). Published by the Royal Society of Chemistry

L. A. Tapondjou, T. Opatz, V. Kuete, R. Kalscheuer, S. F. Kouam and R. B. Teponno, *Nat. Prod. Res.*, 2025, 1–9.
9 N. M. Krstić, M. S. Bjelaković, M. M. Dabović and V. D. Pavlović, *Molecules*, 2010, **15**, 3462–3477.
10 M. P. Savić, D. Đ. Škorić, I. Z. Kuzminac, D. S. Jakimov, V. V. Kojić, L. Rárová, M. Strnad and E. A. Djurendić, *Steroids*, 2020, **157**, 108596.
11 M. Heidary, S. Ghasemi, Z. Habibi and F. Ansari, *Biotechnol. Lett.*, 2020, **42**, 1767–1775.
12 A. Aziz, S. Bano, Atia-tul-Wahab and M. I. Choudhary, *Steroids*, 2020, **154**, 108467.
13 G. D. A. Martin, J. Narvaez and A. Marti, *J. Nat. Prod.*, 2013, **76**, 1966–1969.
14 S. Ramachandra, V. Ramesh, H. Krishnamurthy, N. Kumar, K. Sundaram, M. Hardy and A. Rao, *Reproduction*, 2002, **124**, 301–309.
15 M. J. Walton, N. Kumar, D. T. Baird, H. Ludlow and R. A. Anderson, *J. Androl.*, 2007, **28**, 679–688.
16 A. Clarke, J. Scarth, P. Teale, C. Pearce and L. Hillyer, *Drug Test. Anal.*, 2011, **3**, 74–87.
17 P. J. Stephens, F. J. Devlin and J. J. Pan, *Chirality*, 2008, **20**, 643–663.
18 K. B. Wiberg, Y. Wang, P. H. Vaccaro, J. R. Cheeseman, G. Trucks and M. J. Frisch, *J. Phys. Chem. A*, 2004, **108**, 32–38.
19 N. Berova, L. Di Bari and G. Pescitelli, *Chem. Soc. Rev.*, 2007, **36**, 914–931.
20 G. Pescitelli and T. Bruhn, *Chirality*, 2016, **28**, 466–474.
21 B. Mennucci, J. Tomasi, R. Cammi, J. R. Cheeseman, M. J. Frisch, F. J. Devlin, S. Gabriel and P. J. Stephens, *J. Phys. Chem. A*, 2002, **106**, 6102–6113.
22 P. L. Polavarapu, *Chirality*, 2006, **18**, 348–356.
23 L. A. Nafie, *Vibrational Optical Activity: Principles and Applications*, John Wiley & Sons, Chichester, 2011.
24 L. R. Wiseman and K. L. Goa, *Drugs Aging*, 1996, **9**, 292–306.
25 P. Łyczko, A. Panek and A. Świzdor, *Catalysts*, 2020, **11**, 16.
26 M. Siddiqui, Atia-tul-Wahab, N. Naveed Shaikh, E. Baydoun, Atta-ur-Rahman and M. I. Choudhary, *Phytochem. Lett.*, 2021, **44**, 137–141.
27 B. Y. G. Mountessou, I. L. Mouafon, R. Maharjan, J. Tchamgoue, G. L. M. Tiani, P. Dibouloul, M. I. Choudhary and S. F. Kouam, *RSC Adv.*, 2025, **15**, 25441–25449.
28 A. V. Aksenov, I. Y. Grishin, D. A. Aksenov, Y. I. Grishin, I. V. Aksenova and N. A. Aksenov, *Russ. Chem. Bull.*, 2024, **73**, 1612–1622.
29 V. Crunelli, Z. Emri and N. Leresche, *Curr. Opin. Pharmacol.*, 2006, **6**, 44–52.
30 J. Wildmann, W. Vetter, U. B. Ranalder, K. Schmidt, R. Maurer and H. Möhler, *Biochem. Pharmacol.*, 1988, **37**, 3549–3559.
31 K. Kristan, T. L. Rižner and J. Steroid, *Biochem. Mol. Biol.*, 2012, **129**, 79–91.
32 W. D. Nes, *Chem. Rev.*, 2011, **111**, 6423–6451.
33 S. R. M. Ibrahim, G. A. Mohamed and S. A. Ross, *Phytochem. Lett.*, 2016, **15**, 125–130.
34 K. Trisuwan, N. Khamthong, V. Rukachaisirikul, S. Phongpaichit, S. Preedanon and J. Sakayaroj, *J. Nat. Prod.*, 2010, **73**, 1507–1511.
35 J. Kornsakulkarn, K. Dolsophon, N. Boonyuen, T. Boonruangprapa, P. Rachtawee, S. Prabpai, P. Kongsaeree and C. Thongpanchang, *Tetrahedron*, 2011, **67**, 7540–7547.
36 C.-X. Jiang, J. Li, J.-M. Zhang, X.-J. Jin, B. Yu, J.-G. Fang and Q.-X. Wu, *J. Agric. Food Chem.*, 2019, **67**, 1839–1846.
37 C. Kehelpannala, N. S. Kumar, L. Jayasinghe, H. Araya and Y. Fujimoto, *J. Chem. Ecol.*, 2018, **44**, 95–101.
38 F. Senatore, A. Nunziata, M. D'Agostino and V. De Feo, *Pharm. Biol.*, 1999, **37**, 366–368.
39 S. Woodhead, C. Galeffi and G. B. M. Bettolo, *Phytochemistry*, 1982, **21**, 455–456.
40 M. J. Lee, G. J. Kim, M.-S. Shin, J. Moon, S. Kim, J.-W. Nam, K. S. Kang and H. Choi, *Appl. Sci.*, 2021, **11**, 8866.
41 B. Sun, S. Li, Z.-D. Yang, K.-Z. Ma, Y.-K. Li and X.-Q. Yang, *Chem. Nat. Compd.*, 2025, **61**, 164–168.
42 F. Groß, E. A. Lewis, M. Piraee, K.-H. Van Pée, L. C. Vining and R. L. White, *Bioorg. Med. Chem. Lett.*, 2002, **12**, 283–286.
43 A. Berg, H. V. Kemami Wangun, A. E. Nkengfack and B. Schlegel, *J. Basic Microbiol.*, 2004, **44**, 317–319.
44 A. Doğan, S. Otlu, Ö. Çelebi, P. Aksu Kiliçle, A. Gülmez Sağlam, A. N. C. Doğan and N. Mutlu, *Turk. J. Vet. Anim. Sci.*, 2017, **41**, 302–305.
45 R. Singh and R. Bansal, *RSC Med. Chem.*, 2025, **16**, 2902–2918.
46 I. Z. Kuzminac, M. P. Savić, J. J. Ajduković and A. R. Nikolić, *Curr. Top. Med. Chem.*, 2023, **23**, 791–815.
47 M. S. Elnaggar, N. M. Mostafa, A. M. Elissawy, K. Phutthacharoen, P. Eckhardt, B. Sandargo, L. van Geelen, S. S. Ebada, T. Opatz, A. N. B. Singab and R. Kalscheuer, *Fitoterapia*, 2024, **179**, 106254.
48 J. D. D. Tamokou, A. T. Mbaveng and V. Kuete, in *Medicinal Spices and Vegetables from Africa*, Elsevier, 2017, pp. 207–237.
49 R. Batista, A. De Jesus Silva Júnior and A. B. De Oliveira, *Molecules*, 2009, **14**, 3037–3072.
50 P. D. Douanla, T. K. Tabopda, A. T. Tchinda, E. Cieckiewicz, M. Frédérich, F. F. Boyom, N. Tsabang, S. Yeboah, A. E. Nkengfack and M. H. K. Tchuendem, *Phytochemistry*, 2015, **117**, 521–526.
51 B. S. Sisodia, A. S. Negi, M. P. Darokar, U. N. Dwivedi and S. P. S. Khanuja, *Chem. Biol. Drug Des.*, 2012, **79**, 610–615.
52 J. C. Krug, in *Biodiversity of Fungi*, Elsevier, 2004, pp. 589–593.
53 B. Y. G. Mountessou, E. G. M. Anoumedem, B. M. Kemkuignou, Y. Marin-Felix, F. Surup, M. Stadler and S. F. Kouam, *Beilstein J. Org. Chem.*, 2023, **19**, 1555–1561.
54 C. Bannwarth, S. Ehlert and S. J. Grimme, *J. Chem. Theory Comput.*, 2019, **15**, 1652–1671.
55 P. Pracht, S. Grimme, C. Bannwarth, F. Bohle, S. Ehlert, G. Feldmann, J. Gorges, M. Müller, T. Neudecker, C. Plett, S. Spicher, P. Steinbach, P. A. Wesołowski and F. Zeller, *J. Chem. Phys.*, 2024, **160**, 114110.
56 F. Weigend and R. Ahlrichs, *Phys. Chem. Chem. Phys.*, 2005, **7**, 3297–3305.

© 2026 The Author(s). Published by the Royal Society of Chemistry

57 F. Weigend, *Phys. Chem. Chem. Phys.*, 2006, **8**, 1057–1065.
58 S. Grimme, J. Antony, S. Ehrlich and H. Krieg, *J. Chem. Phys.*, 2010, **132**, 154104.
59 M. J. Frisch, G. W. Trucks, H. B. Schlegel *et al.*, *Gaussian 16, Revision C.01*, Gaussian, Inc., Wallingford CT, 2016.
60 T. Bruhn, A. Schaumlöffel, Y. Hemberger and G. Bringmann, *Chirality*, 2013, **25**, 243–249.
61 N. Gallagher, *Savitzky-Golay Smoothing and Differentiation Filter*, 2020.
62 W. Trager and J. B. Jensen, *Science*, 1976, **193**, 673–675.
63 C. Lambros and J. P. Vanderberg, *J. Parasitol.*, 1979, **65**, 418–420.
64 K. Kirk, H. A. Horner, B. C. Elford, J. C. Ellory and C. I. Newbold, *J. Biol. Chem.*, 1994, **269**, 3339–3347.
65 M. Smilkstein, N. Sriwilaijaroen, J. X. Kelly, P. Wilairat and M. Riscoe, *Antimicrob. Agents Chemother.*, 2004, **48**, 1803–1806.
66 S. Sinha, D. I. Batovska, B. Medhi, B. D. Radotra, A. Bhalla, N. Markova and R. Sehgal, *Malar. J.*, 2019, **18**, 421.

© 2026 The Author(s). Published by the Royal Society of Chemistry